A hyperspectral image endmember extraction algorithm based on generalized morphology*

WANG Dong-hui (王东辉)[1], YANG Xiu-kun (杨秀坤)[1], and ZHAO Yan (赵岩)[2]**

1. College of Information and Communication Engineering, Harbin Engineering University, Harbin 150001, China

2. Electric and Control Engineering College, Heilongjiang University of Science and Technology, Harbin 150022, China

(Received 20 May 2014)

Generalized morphological operator can generate less statistical bias in the output than classical morphological operator. Comprehensive utilization of spectral and spatial information of pixels, an endmember extraction algorithm based on generalized morphology is proposed. For the limitations of morphological operator in the pixel arrangement rule and replacement criteria, the reference pixel is introduced. In order to avoid the cross substitution phenomenon at the boundary of different object categories in the image, an endmember is extracted by calculating the generalized opening-closing (GOC) operator which uses the modified energy function as a distance measure. The algorithm is verified by using simulated data and real data. Experimental results show that the proposed algorithm can extract endmember automatically without prior knowledge and achieve relatively high extraction accuracy.

Document code: A **Article ID:** 1673-1905(2014)05-0387-4

DOI 10.1007/s11801-014-4088-5

Hyperspectral imaging technology is widely used for remote sensing to obtain the spatial and spectral domain information simultaneously by collecting dozens or even hundreds of bands of spectral data from the same surface area using spectrometer[1-3]. Earth's natural surface is rarely composed of homogenous materials. When the same pixel contains different spectral properties of the material, it can be referred to mixed pixel[4-6]. Endmember extraction is necessary before mixed pixel decomposition in linear mixed model[7]. The endmember as prior knowledge of mixed pixel decomposition is obtained[8]. Endmember spectrum is used as reference spectrum in the process of decomposition of mixed pixels and directly affects the precision of the results of decomposition of mixed pixels[9]. The commonly used methods for acquiring endmember spectrum are pure pixel index (PPI), N-FINDR algorithm, vector component analysis (VCA), iterative error analysis (IEA), etc. These methods only consider the spectral information, while ignor the spatial correlation between pixels[10]. Automated morphological endmember extraction (AMEE)[11,12] is introduced to reflect the morphological operator space correlation information between pixels in the hyperspectral image processing, and its endmember extraction performance is enhanced. Dilation operation in AMEE is applied to the boundary of different object categories in the image, and the phenomenon of cross substitution occurs. For the limitations existing in AMEE algorithm, the calculating method for the key parameter, i.e., reference pixel, is presented, and the modified energy function (EF) of the regularization is introduced. The endmember is extracted by calculating the generalized morphological opening-closing operator which uses modified EF as distance measure. The proposed algorithm is hereafter referred to the generalized morphological end-member extraction (GMEE). Simulation results demonstrate that the proposed method can precisely extract the endmember.

The EF, which is used for the energy measurement of adjacent pixels[13], contains space comparative information of image. Considering the N dimensional spectral vectors $\boldsymbol{s}_i=[s_{i1}, s_{i2},\cdots, s_{iN}]^{\mathrm{T}}$ and $\boldsymbol{s}_j=[s_{j1}, s_{j2},\cdots, s_{jN}]^{\mathrm{T}}$, EF of $\boldsymbol{s}_i$ and $\boldsymbol{s}_j$ can be represented as

$$EF(\boldsymbol{s}_i,\boldsymbol{s}_j)=dist_2^{-1}(\boldsymbol{s}_i,\boldsymbol{s}_j)\exp[-dist_1^2(\boldsymbol{s}_i,\boldsymbol{s}_j)]\,, \tag{1}$$

where $dist_1$ is the mixed distance, namely $dist_1(\boldsymbol{s}_i,\boldsymbol{s}_j)=\sum_{k=1}^{N}\left|s_{ik}-s_{jk}\right|$, and $dist_2$ is the Euclidean distance, namely $dist_2(\boldsymbol{s}_i,\boldsymbol{s}_j)=[\sum_{k=1}^{N}(s_{ik}-s_{jk})^2]^{\frac{1}{2}}$.

Some of the commonly used measures to characterize the two spectral similarity distance measures include the spectral angle distance (SAD), Euclidean minimum distance (EMD), spectral information divergence (SID), mahalanobis distance (MD), etc. Modified energy func-

* This work has been supported by the National Natural Science Foundation of China (No.61275010), and the PhD Programs Foundation of Ministry of Education of China (No.20132304110007).

** E-mail: wangdonghui@hrbeu.edu.cn

tion (MEF) is introduced to calculate the distance. Euclidean distance $dist_2$ in the EF is replaced by Mahalanobis distance $dist_3$ with the regularization term. The regularization term is added into the covariance matrix, which can improve the stability of calculation of the inverse matrix of covariance matrix and is suitable for smaller samples[14]. There is a complex correlation between pixel spectral bands. Mahalanobis distance not only considers the distance between spectra, but also can eliminate the interference of the correlation between spectral bands. Therefore, the effect of Mahalanobis distance as the distance measure is better than that of Euclidean distance. MEF can be written as

$$MEF(\boldsymbol{s}_i,\boldsymbol{s}_j)=dist_3^{-1}(\boldsymbol{s}_i,\boldsymbol{s}_j)\exp[-dist_1^2(\boldsymbol{s}_i,\boldsymbol{s}_j)], \qquad (2)$$

where the Mahalanobis distance with the regularization term is $dist_3(\boldsymbol{s}_i,\boldsymbol{s}_j)=\{(\boldsymbol{s}_i-\boldsymbol{s}_j)^{\mathrm{T}}[\mathrm{cov}(\boldsymbol{s}_i,\boldsymbol{s}_j)+\lambda\boldsymbol{I}]^{-1}(\boldsymbol{s}_i-\boldsymbol{s}_j)\}^{\frac{1}{2}}$, λ is regularization coefficient, which is a very small positive number, $\boldsymbol{I}$ is a unit matrix, and cov(a, b) is covariance.

Mathematical morphology which was founded by the French mathematician G. Matheron and J. Serra in the mid-1960s is a nonlinear image processing technology based on the lattice theory and topology. The size and shape of structural elements both affect the spatial information extraction of morphology image[15]. Compared with classical morphological operator, the generalized morphological operator uses two structure elements with different sizes to generate less statistical bias in the output[16], and thus improves endmember extraction performance. Generalized morphological operator can process the whole spectral vector[17]. The generalized opening-closing (GOC) operator and the generalized closing-opening (GCO) operator can be written as[18]

$$GOC_{MEF}(\boldsymbol{f}(x,y))=(\boldsymbol{f}\mathrm{o}\boldsymbol{B}_1\mathrm{g}\boldsymbol{B}_2)_D(x,y), \qquad (3)$$

$$GCO_{MEF}(\boldsymbol{f}(x,y))=(\boldsymbol{f}\mathrm{g}\boldsymbol{B}_1\mathrm{o}\boldsymbol{B}_2)_D(x,y), \qquad (4)$$

where o is morphological opening operation, g is morphological closing operation, $\boldsymbol{f}(x, y)$ is N dimensional spectral vector, and (x, y) is space coordinates. $\boldsymbol{B}_1$ and $\boldsymbol{B}_2$ are structure elements, and space size of $\boldsymbol{B}_2$ is bigger than that of $\boldsymbol{B}_1$. $D(\boldsymbol{f}(x,y),\boldsymbol{B}_i)=MEF(\boldsymbol{f}(x,y),\boldsymbol{C}_{\boldsymbol{B}_i})$, $\boldsymbol{C}_{\boldsymbol{B}_i}=\frac{1}{M}\sum_s\sum_t\boldsymbol{f}(s,t)$, $\forall(s,t)\in\boldsymbol{B}_i$, i=1, 2, M is the number of pixels in structure elements $\boldsymbol{B}_i$.

In general, the GOC_{MEF} value of pure pixel is the maximum and GOC_{MEF} is approximately equal to zero, while the GOC_{MEF} value of mixed pixel is the maximum and GOC_{MEF} is approximately equal to zero.

AMEE algorithm extracts pure pixel and mixed pixel by dilation and erosion operations. However, the dilation operation can not guarantee that the pure pixel covers the mixed pixel, and the erosion operation can not guarantee that the mixed pixel covers the pure pixel, since the vector with the maximum distance in the dilation operation of structural element is often the most isolated spectral vector in spectral feature space, rather than pure pixels. Similarly, the vector with the mininum distance in the erosion operation of structural element is the central spectral vector of data cloud in spectral feature space. Therefore, when the dilation operation is applied on the boundary of different object categories in the image, the phenomenon of cross substitution occurs, namely, grating effect[19]. In order to avoid cross substitution phenomenon, the reference pixel is introduced. The pixel vector with maximum value of GOC_{MEF} is defined as the reference pixel, which is located in the center of data cloud in spectral feature space. The substitution rule of pixel in structure element is modified on the basis of GOC_{MEF}. The modified GOC'_{MEF} is expressed as

$$GOC'_{MEF}(\boldsymbol{f}(x,y))=(\boldsymbol{f}\mathrm{o}\boldsymbol{B}_1\mathrm{g}\boldsymbol{B}_2)_{D'}(x,y), \qquad (5)$$

where $D'(\boldsymbol{f}(x,y),\boldsymbol{B}_i)=MEF(\boldsymbol{f}(x,y),\boldsymbol{e}(j,k))$, and the reference pixel $\boldsymbol{e}(j, k)$ can be expressed as

$$\boldsymbol{e}(j,k)=\arg\min((\boldsymbol{f}\mathrm{g}\boldsymbol{B}_1\mathrm{o}\boldsymbol{B}_2)_D(x,y)). \qquad (6)$$

Endmember extraction steps are described as follows. (1) Use the method of virtual dimensionality (VD)[20] to estimate the number of endmembers as the termination condition of the algorithm. When the number of extracted endmembers reaches the estimated number of endmembers, the operation is ended. (2) Set space sizes of structure elements $\boldsymbol{B}_1$ and $\boldsymbol{B}_2$. (3) Compute the reference pixel $\boldsymbol{e}(j, k)$ in the whole image. (4) Calculate GOC'_{MEF} on each pixel in the image used for endmember extraction. (5) Put the pixel of the maximum value of GOC'_{MEF} as endmember. (6) Set GOC'_{MEF} of similar pixels of the acquired endmember to zero in order to eliminate the effect of the acquired endmember. (7) Repeat step (4) if the termination condition of step (1) is not satisfied.

The SAD is used to measure the accuracy.

For the ith endmember, SAD is defined as

$$SAD_i=\cos^{-1}\left(\frac{\boldsymbol{S}_i^{\mathrm{T}}\hat{\boldsymbol{S}}_i}{\left\|\boldsymbol{S}_i^{\mathrm{T}}\right\|\left\|\hat{\boldsymbol{S}}_i\right\|}\right), \qquad (7)$$

where $\boldsymbol{S}$ is the true endmember spectrum, and $\hat{\boldsymbol{S}}$ is estimated value of $\boldsymbol{S}$.

Four linearly independent endmember spectra (alunite, buddingtonite, calcite and kaolinite) are selected from United States Geological Survey (USGS) mineral spectral library and mixed according to the Dirichlet distribution and the normalization of sum of endmember abundances. Different white noises are added to generate the simulation experimental data. The number of bands is 50, and the image size is 256 pixel × 256 pixel.

Fig.1 shows the performance evaluation of the endmember extraction by GMEE, AMEE and VCA algorithms under different signal to noise ratios (SNRs). The anti-noise experiments are performed at SNR of ∞ (without noise), 30 dB, 20 dB and 10 dB, respectively. GMEE algorithm uses the square structure elements of $\boldsymbol{B}_1(3\times3)$ and $\boldsymbol{B}_2(5\times5)$. $\overline{SAD}$ represents the mathematical expectation of *SAD*. It can be seen from Fig.1 that when the SNR decreases, the results of three kinds of algorithms get worse. The performance of GMEE algorithm is better than that of the other two algorithms in terms of endmember extraction.

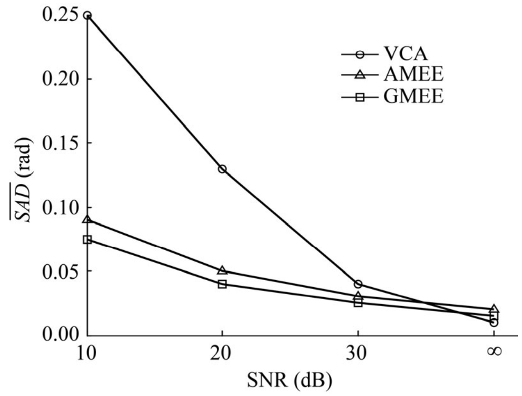

Fig.1 Performance of the endmember extraction by GMEE, AMEE and VCA algorithms at different noise intensities

The real hyperspectral image data collected by airborne visible/infrared imaging spectrometer (AVIRIS) in 1995 for cuprite mining district of Nevada in United States is used for performance evaluation. As shown in Fig.2, the image containing 400 pixel×350 pixel and 50 bands (1.99–2.48 μm) ranging from 172 to 221. 49 bands is used in the experiment, and the atmospheric absorption band of 221 is removed. The actual image size is 13.3 MB.

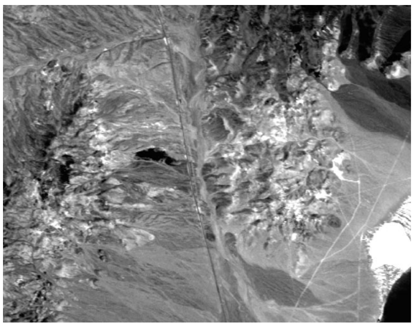

Fig.2 AVIRIS image data in cuprite region (183 band)

GMEE algorithm uses the square structure elements of $\boldsymbol{B}_1(3\times3)$ and $\boldsymbol{B}_2(5\times5)$. Tab.1 gives the similarity between the endmembers of 5 kinds of common minerals in cuprite region and the reference spectra of their actual corresponding objects by GMEE, AMEE and VCA algorithms. As can be seen from Tab.1, compared with the other two algorithms, GMEE algorithm which makes full use of the spatial and spectral information further improves the purity of the extracted endmember by using the generalized morphological methods.

Tab.1 Comparison for the cuprite dataset

Algorithm	Alunite	Buddingtonite	Calcite	Kaolinite	Muscovite	Average similarity
GMEE	0.042	0.121	0.125	0.069	0.068	0.085
AMEE	0.052	0.136	0.145	0.070	0.071	0.094
VCA	0.089	0.108	0.138	0.234	0.078	0.142

In this paper, based on the study of AMEE algorithm, an endmember extraction method of hyperspectral image is proposed based on generalized morphological operator. In order to ensure the correct replacement, the reference pixel is introduced, and the MEF is used as the distance measure from the pixel arrangement rule and replacement criteria in structural elements. The GMEE algorithm is proposed by combining the spectral and spatial information, and the correlation of spectral bands is considered. The experimental analysis by simulated data and real data indicates that the proposed method can improve the accuracy of endmember extraction.

References

[1] Cheng bao-zhi and Zhao chun-hui, Journal of Optoelectronics·Laser **24**, 2047 (2013). (in Chinese)

[2] Lv Zeng-ming, Li Jin, Tao Hong-jiang, Jin long-xu and Zhang Ran-feng, Journal of Optoelectronics·Laser **23**, 2027 (2012). (in Chinese)

[3] Cheng bao-zhi, Zhao chun-hui and Wang Yu-lei, Journal of Optoelectronics·Laser **23**, 1582 (2012). (in Chinese)

[4] Yokoya N., Chanussot J. and Iwasaki A., IEEE Transactions on Geoscience and Remote Sensing **52**, 1430 (2014).

[5] Ambikapathi A., Chan Tsung-Han, Chi Chong-Yung and Keizeer K., IEEE Transactions on Geoscience and Remote Sensing **51**, 2753 (2013).

[6] Heylen R., Burazerovic D. and Scheunders P., IEEE Journal on Selected Topics in Signal Processing **5**, 534 (2011).

[7] Neville R. A., Staenz K., Szeredi T., Lefebvre J. and Hauff P., Automatic Endmember Extraction from Hyperspectral Data for Mineral Exploration, 21st Canadian Symposium on Remote Sensing, 21 (1999).

[8] Wang Liguo and Zhao Chunhui, Processing Techniques of Hyperspectral Imagery, Beijing: National Defense Industry Press, 11 (2013). (in Chinese)

[9] Deng Shu-bin, ENVI Remote Sensing Image Processing Method, Beijing: Science Press, 334 (2010). (in Chinese)

[10] Rongrong Ji, Yue Gao, Richang Hong, Qiong Liu, Dacheng Tao and Xuelong Li, IEEE Transactions Geoscience and Remote Sensing **52**, 1811 (2014).

[11] Plaza A., Martinez P., Perez R. and Plaza J., IEEE Transactions Geoscience and Remote Sensing **40**, 2025 (2002).

[12] Du Peijun, Tan Kun and Xia Junshi, Hyperspectral Remote Sensing Image Classification and Application Research on Support Vector Machine, Beijing: Science Press, 135 (2012). (in Chinese)

[13] Sun Xian, Fu Kun and Wang Hongqi, High Resolution Remote Sensing Image Understanding, Beijing: Science Press, 145 (2011). (in Chinese)

[14] Nasser M. Nasrabadi, Regularization for Spectral Matched Filter and RX Anomaly Detector, Proc. SPIE **6966**, 696604 (2008).

[15] Liu Sheng, Wang Xiaoyu and Qiu Xinfa, Meteorology and Disaster Reduction Research **31**, 48 (2008). (in Chinese)

[16] Duan Shan, Mathematica Morphology and its Application Research in Remote Sensing Image Processing, Wuhan: Wuhan Univesity, 115 (2004).

[17] Plaza A., Martinez P., Plaza J. and Perez R., IEEE Transactions on Geoscience and Remote Sensing **43**, 466 (2005).

[18] Zhao Chunhui, Research on Digital Morphological Filter Theory and its Algorithms, Heilongjiang: Harbin Institute of Technology, 59 (1998).

[19] Wang Ying, Liang Nan and Guo Lei, Acta Photonica sinica **41**, 672 (2012). (in Chinese)

[20] Chang Chein-I and Du Qian, IEEE Transactions on Geoscience and Remote Sensing **42**, 608 (2004).